Journal of proteome research

pubs.acs.org/jpr

Article

Quantitative Proteomics Reveals Docosahexaenoic Acid-Mediated Neuroprotective Effects in Lipopolysaccharide-Stimulated Microglial Cells

Bo Yang, Runting Li, Pei N. Liu, Xue Geng, Brian P. Mooney, Chen Chen, Jianlin Cheng, Kevin L. Fritsche, David Q. Beversdorf, James C. Lee, Grace Y. Sun, and C. Michael Greenlief*

Cite This: J. Proteome Res. 2020, 19, 2236−2246

Read Online

ACCESS | Metrics & More | Article Recommendations | Supporting Information

ABSTRACT: The high levels of docosahexaenoic acid (DHA) in cell membranes within the brain have led to a number of studies exploring its function. These studies have shown that DHA can reduce inflammatory responses in microglial cells. However, the method of action is poorly understood. Here, we report the effects of DHA on microglial cells stimulated with lipopolysaccharides (LPSs). Data were acquired using the parallel accumulation serial fragmentation method in a hybrid trapped ion mobility-quadrupole time-of-flight mass spectrometer. Over 2800 proteins are identified using label-free quantitative proteomics. Cells exposed to LPSs and/or DHA resulted in changes in cell morphology and expression of 49 proteins with differential abundance (greater than 1.5-fold change). The data provide details about pathways that are influenced in this system including the nuclear factor κ-light-chain-enhancer of the activated B cells (NF-κB) pathway. Western blots and enzyme-linked immunosorbent assay studies are used to help confirm the proteomic results. The MS data are available at ProteomeXchange.

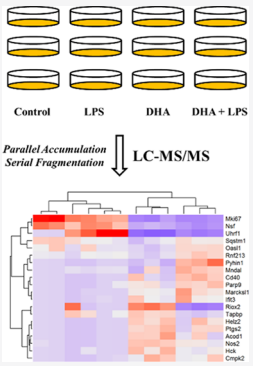

KEYWORDS: *docosahexaenoic acid, microglia, lipopolysaccharide, label-free quantification, ion mobility, TIMS, time-of-flight*

1. INTRODUCTION

Phospholipids in the central nervous system (CNS) are enriched in docosahexaenoic acid (22:6(n-3), DHA). To-date, n-3 PUFAs in the form of fish oil are one of the most highly consumed dietary supplements by humans. Because of its diverse functions, a growing body of studies have suggested the impact of DHA and related metabolites to exert anti-inflammatory and insulin-sensitizing effects in cells, thus mitigating the progression of inflammatory diseases.[1−3]

Microglial cells, the resident immune cells in the CNS, are recognized as an important cellular sentinel of inflammatory responses in the brain.[4−6] These cells are highly dynamic and exhibit a complex spectrum of pathways with multiple phenotypes affected by exogenous and endogenous factors.[7] Our recent studies demonstrated similarities in inflammatory responses between primary microglial cells isolated from the mouse brain and the murine immortalized BV-2 microglial cells.[8] Subsequently, BV-2 microglial cells became a good model for studies to investigate the biochemical profiles of inflammatory and oxidative pathways.[8−13] In a recent quantitative proteomics study using an orbitrap mass spectrometer, information about proteomic changes in signaling pathways upon stimulation of BV-2 cells with lipopolysaccharides (LPSs) and interferon-γ were investigated.[14] That study showed that activation of microglial cells was associated with the toll-like receptor (TLR) signaling and increases in oxidation and inflammatory responses at the proteome level. In addition, a global-scale proteomics study successfully defined proteins associated with different phenotypic expressions of microglial activation, ranging from M1 to M2a, M2b, and M2c stages.[15] Considering that activation of microglia plays an important role in different neuroinflammatory diseases, it is of importance to understand factors that mitigate microglial activation.[16−18]

Despite high levels of DHA and arachidonic acid (20:4(n-6), ARA) in phospholipids in the brain, there is evidence that these two PUFAs are engaged in distinctly different physiological functions, largely because of different types of phospholipases A_2 (PLA_2s) mediating their release from membrane phospholipids.[19−21] ARA is released by cytosolic PLA_2 ($cPLA_2$), and is metabolized by cyclooxygenases (COX) and lipoxygenases (LOX) to form eicosanoids, lipid mediators that are largely associated with inflammation. In contrast, release of DHA by the calcium-independent PLA_2 ($iPLA_2$) is linked to synthesis of pro-resolving oxylipins through interaction with ALOX15.[22,23] A study with HT-29 colorectal cancer cells showed significant differences in functions between DHA and ARA at the proteome level.[24] Our recent study on microglial cells also demonstrated

Received: December 3, 2019
Published: April 17, 2020

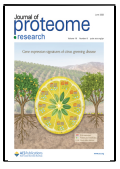

https://dx.doi.org/10.1021/acs.jproteome.9b00792
J. Proteome Res. 2020, 19, 2236−2246

the effects of DHA to inhibit LPS-induced oxidative and inflammatory responses, including the NF-κB and the cPLA$_2$/ARA pathways.[13] However, investigations are needed to further examine the multiple effects of DHA against microglial activation at the proteome level. Ion mobility spectrometry is a relatively new separation method, and when used in combination with hybrid mass spectrometers, can provide a powerful addition to proteomics.[25] Compared to the orbitrap-based methods, studies utilizing parallel accumulation serial fragmentation (PASEF) in trapped ion mobility spectrometry (TIMS) for proteome quantification have demonstrated technical advantages, in both accuracy and reliability of protein quantification, as well as increased identification of low-abundance proteins.[26,27]

In this study, we performed label-free quantitative proteomics to test the effects of LPS and/or DHA on BV-2 microglial cells. Results identified differentially abundant proteins (DAPs) and their corresponding pathways. In order to verify proteomic changes, the study included supporting data including cell morphology, viability, Western blot analysis, and enzyme-linked immunosorbent assays (ELISAs). The results of the proteomic study provided firm evidence regarding the multiple protective effects of DHA on activated microglial cells, and further shed light on the complex molecular mechanisms underlying the effects of DHA and/or LPS on proteomes in microglial cells.

2. MATERIALS AND METHODS

2.1. Materials and Reagents

Docosahexaenoic acid (DHA, 100 mg in 0.4 mL of ethanol) and prostaglandin E2 (PGE2) ELISA kit (#514010) were purchased from Cayman Chemical (Ann Arbor, MI). Dithiothreitol (DTT), iodoacetamide (IAA), fetal bovine albumin (FBS), formic acid (FA, mass spectrometry grade), and monoclonal anti-β-actin peroxidase (#A3854) were purchased from Sigma-Aldrich (St. Louis, MO). The WST-1 assay kit was obtained from Clontech (Mountain View, CA). Dulbecco's modified Eagle's medium (DMEM) and penicillin/streptomycin were obtained from Life Technologies (Grand Island, NY). Antibodies of phospho-NF-κB p65 (Rabbit mAb #3033) and NF-κB p65 (Rabbit mAb #8242) were from Cell Signaling (Beverly, MA). Anti-inducible nitric oxide synthase (iNOS) (#ab15323) was from Abcam (Cambridge, MA). Urea (electrophoresis grade), thiourea (electrophoresis grade), sodium dodecyl sulfate (SDS), ammonium bicarbonate, BCA protein assay kit, EZQ protein assay kit, SuperSignal west pico plus chemiluminescent substrate, Restore PLUS Western blot stripping buffer, tumor necrosis factor α (TNF-α) mouse uncoated ELISA kit (#88-7324-88), C_{18} tips, dimethyl sulfoxide (DMSO), water (H_2O, HPLC grade), and acetonitrile (ACN, HPLC grade) were obtained from Thermo Fisher (Waltham, MA). Modified porcine trypsin was acquired from Promega (Madison, WI).

2.2. Cell Culture and Treatments

BV-2 microglial cells were originally obtained from R. Donato (University of Perugia, Italy), and subsequently maintained in G. Sun's laboratory as previously described.[28] Briefly, cells were cultured in 75 cm^2 flasks with DMEM supplemented with 5% FBS, and 100 units/mL penicillin and streptomycin (100 μg/mL), and maintained in a 5% CO_2 incubator at 37 °C. For proteomic analysis, cells were subcultured in 12-well plates; for morphology experiments, cells were subcultured in 35 mm dishes; for WST-1 experiments, cells were subcultured in 96-well plates; and for TNF-α, phospho-NF-κB p65, iNOS, and PGE2 experiments, cells were subcultured in six-well plates. In all conditions, cells were subcultured to 80−90% confluence and then serum starved for 3 h prior to adding DHA (20 μM) for 1 h, followed by stimulation with or without LPS (100 ng/mL) for 16 h. For each treatment condition, three biological replicates were used for the proteomics study. DHA was initially dissolved in DMSO and further diluted in DMEM to a final concentration of 20 μM. Controls were treated with the same dilution of DMSO in DMEM.

2.3. Assessment of Cell Viability and Morphology

Cell viability was determined using the WST-1 kit as previously described.[13] Briefly, after treatment conditions, WST-1 was added to each well with medium/WST-1 reagent at 15:1 (v/v). Cells were incubated for 1 h at 37 °C, and after dissolving the formazan dye with DMSO, absorption was read at 450 nm using a Synergy4 Plate Reader (BioTek Instruments, Inc., Winooski, VT).

Assessment of cell morphology was performed as previously described.[29] Cells were examined using a phase contrast Nikon Diaphot 300 microscope attached with a CCD cooled camera. Images were obtained with the magnification at 20× and the microscope was linked to MagnaFire 2.1C software for image processing. Normally, three to four bright field pictures of cells from triplicate experiments with different passages were captured from each dish.

2.4. Quantification of TNF-α and PGE2 by ELISA

Previous studies demonstrated the ability for LPSs to stimulate release of TNF-α and PGE2 from microglial cells, mainly through activation of the NF-κB and the cPLA2/ARA/COX2 pathways.[8] In this study, the concentrations of TNF-α and PGE2 in cell supernatants were determined using an ELISA protocol. Briefly, after culturing cells with different conditions, the culture media was obtained and centrifuged at 4000*g* for 5 min to remove cell debris. The supernatant was obtained for ELISAs of TNF-α and PGE2 as previously described.[8,12] The remaining cells were lysed with RIPA buffer and saved for protein determination using the BCA assay. TNF-α values were read and analyzed at 450 nm and PGE2 values at 410 nm after subtracting the respective backgrounds.

2.5. Western Blot Analysis of iNOS and Phospho-NF-κB p65

In this study, Western blot analyses of phospho-p65 (subunit of the NF-κB complex) and the iNOS protein were used to examine the effects of LPSs and/or DHA on the NF-κB pathway in microglial cells. After different incubation conditions, cells were lysed in RIPA buffer with protease and phosphatase inhibitors. Cell lysates were centrifuged at 14,000*g* for 15 min at 4 °C to remove cell debris. The protein concentration was measured and normalized by using the BCA assay kit. The same amount of total protein was loaded in SDS-PAGE for electrophoresis, and afterward, proteins were transferred to PVDF membranes at 100 V for 1 h. The membranes were then incubated in Tris-buffered saline with 0.1% Tween 20 (TBS-T) containing 5% nonfat milk for 1 h at room temperature. The blots were incubated with antibodies of iNOS (1:200 dilution), phospho-NF-κB p65 (1:1000 dilution), NF-κB p65 (1:1000 dilution), β-actin (1:50,000 dilution) overnight at 4 °C. After washing with TBS-T, the blots were incubated with antirabbit IgG (1:1000 dilution) for 1 h at room temperature. Immunolabeling was detected by SuperSignal with the pico plus chemiluminescent substrate.

https://dx.doi.org/10.1021/acs.jproteome.9b00792
J. Proteome Res. 2020, 19, 2236−2246

2.6. Statistical Analysis for Cell Viability

Results for cell viability, TNF-α, phospho-NF-κB p65, iNOS, and PGE2 were expressed as the mean ± standard deviation (SD) and analyzed by one-way ANOVA followed by Tukey's post-tests (version 8.01; GraphPad Prism Software, San Diego, CA). Differences were considered significant at a p-value < 0.05 for all analyses.

2.7. Preparation of Cell Lysate for MS

After different treatment conditions, cells were harvested in a buffer solution (4% SDS, 50 mM Tris buffer), followed by incubation at 95 °C for 5 min. The cell lysates were sonicated for 15 min, and then centrifuged for 15 min at 4 °C. The supernatants were transferred to new centrifuge tubes with four volumes of precipitation solution (100% acetone) and stored at −80 °C overnight.[30] The precipitate was washed three times with cold 80% acetone and then resuspended with 6 M urea, 2 M thiourea, and 100 mM ammonium bicarbonate. The EZQ protein assay was conducted as per the manufacturer's instructions. The protein extract was reduced with 200 mM DTT for 60 min at room temperature and alkylated with 200 mM IAA for an additional 60 min in the dark. After alkylation, an excess of 200 mM DTT was added to neutralize the remaining IAA for 60 min. The urea concentration was reduced to 0.6 M by adding Milli-Q water. In-solution digestion was performed with trypsin (1:50, w/w) overnight at 37 °C. The reaction was stopped by the addition of FA to 1% (v/v), and desalted with a C_{18} reversed-phase tips. Samples were stored at −80 °C until use. Triplicate samples of each condition (biological replicates) were collected.

2.8. LC−MS/MS Analysis

A Bruker nanoElute UHPLC system was coupled to a hybrid TIMS-quadrupole time-of-flight mass spectrometer (tims-ToF Pro, Bruker Daltonics, Billerica, MA) with a modified nano-electrospray ion source.[31] A given peptide mixture (800 ng) was reconstituted in 0.1% FA and 5% ACN, and loaded onto a C_{18} reverse phase capillary column (IonOpticks, 75 μm × 150 mm, 1.9 μm) with a constant flow rate of 400 nL/min. Mobile phases A and B were water with 0.1% FA (v/v) and ACN with 0.1% FA (v/v), respectively. Peptides were separated with a linear gradient from 3 to 30% B within 65 min, followed by an increase to 50% B within 10 min and further to 80% B within 7.5 min, and reequilibration.

MS and MS/MS spectra were recorded from m/z 100 to 1700 Da. Proteome coverage was achieved using the PASEF[27] mode. During the MS/MS data collection, each duty cycle included 1 TIMS-MS and an average of 10 PASEF scans. The data were acquired with a 100 ms ramp time, and the quadrupole isolation width was set to 2 Da. TIMS and MS operations were controlled and synchronized using the Bruker OTOF Control software (version 3.2, Bruker Daltonics, Billerica, MA).

2.9. Protein Identification Using PEAKS DB

Raw data were processed using Peaks Studio (version 8.5, Bioinformatics Solutions, Inc., Waterloo, ON). Data were searched against the Uniprot/Swissprot house mouse (*Mus musculus*) protein database (June 2018; 16,977 total entries). The searches were performed with the following guidelines: trypsin as enzyme, two missed cleavages allowed; carbamidomethyl cysteine as a fixed modification; oxidized methionine and deamidation of asparagine and glutamine as variable modification; maximum three variable PTMs per peptide; 50 ppm mass error tolerance on precursor ions; 0.1 Da mass error tolerance on fragment ions. Data were filtered with a peptide match of 0.1% false discovery rate (FDR) with at least one unique peptide required for protein identification. The Peaks Studio software used a decoy fusion method to calculate FDR as published.[32] The program (Peaks Studio) adopts the Benjamin−Hochberg method to adjust the p-value to the FDR for all protein groups that have already passed the other filters. Only protein groups with significance scores passing the calculated FDR are listed in the "Protein" list.

2.10. Protein Quantification and Functional Analysis

DAPs were calculated in R using spectral counts and the following criteria: a first pass analysis was conducted yielding 65 proteins as the differential abundant using one-way ANOVA and a $p < 0.01$, with >1 spectral counts per protein (group average) and in >2 replicates per group.

To further filter the DAP data for significance, a Benjamini−Hochberg FDR correction was conducted yielding 26 proteins (adjusted $p < 0.05$) as significantly changed across the four groups. Finally, correcting for >2 spectral counts (average per group) yielded 20 DAPs, which were graphed as a heatmap in R using the complete clustering method and a pairwise correlation distance method. Database for Annotation, Visualization and Integrated Discovery (DAVID)[33] was used for gene ontology (GO) enrichment analysis of DAPs with the whole *M. musculus* genome as the background and with a significant enrichment threshold of a Benjamini correction of $p < 0.05$. A bubble plot representing these data was generated using R. The DAPs were also subjected to protein−protein interactions (PPI) analysis using the STRING database[34] and Cytoscape software[35] V3.7.0.

2.11. Data Availability

The MS data were deposited at the ProteomeXchange Consortium[36] via the PRIDE partner repository, and are available with the identifier PXD013086.

3. RESULTS AND DISCUSSION

3.1. DHA Pretreatment Attenuates LPS-Induced Morphology Changes in BV-2 Cells

Prior to the proteomics study, we first examined the cell morphology under treatment with DHA (20 μM) and LPSs (100 ng/mL). Similar to observations described in our previous studies,[37] representative photomicrographs of control cells taken at 6 h showed oblong or triangular shaped cells with bright refringence, whereas cells after LPS treatment showed extensive processes (Figure 1A). Whereas DHA pretreatment resulted in more small round cells, DHA pretreatment decreased the processes induced by LPSs (Figure 1A). When cells were cultured for 16 h, many control cells became round, whereas LPS-treated cells were flat with rugged edges and enlarged nuclei surrounded with cytoplasmic inclusions, and some nuclei showed multiple nucleoli (Figure 1B). Whereas DHA pretreatment did not show obvious differences compared with controls, DHA partially minimized the changes because of LPSs (Figure 1B). In these studies, an assay with WST-1 showed that LPS treatment did not alter cell viability (Supplemental Material S1—Figure S1). Based on these data, a 16 h incubation time was used for subsequent proteomics analysis.

3.2. Global Protein Alterations in Cells Exposed to DHA and/or LPSs

On the basis of PASEF scans, 265373 peptide-spectrum matches (PSMs) and 22151 unique peptide sequences were identified from the raw data and were employed for quantitation (FDR of

https://dx.doi.org/10.1021/acs.jproteome.9b00792
J. Proteome Res. 2020, 19, 2236−2246

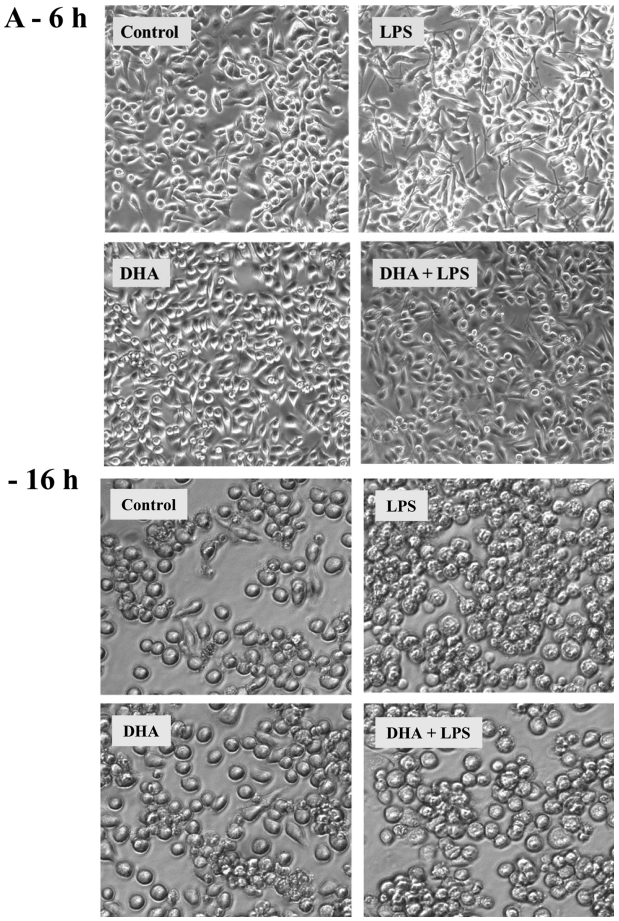

Figure 1. Effects of DHA and/or LPSs on morphology. BV-2 microglial cells were cultured in 35 mm dishes or 96-well plates until reaching 90% confluence. After being serum-starved for 3 h, DHA (20 μM) was added for 1 h and cells were incubated for (A) 6 and (B) 16 h. Representative bright field microscopy images of cells without LPSs and DHA (control), DHA, LPSs, and DHA and LPSs.

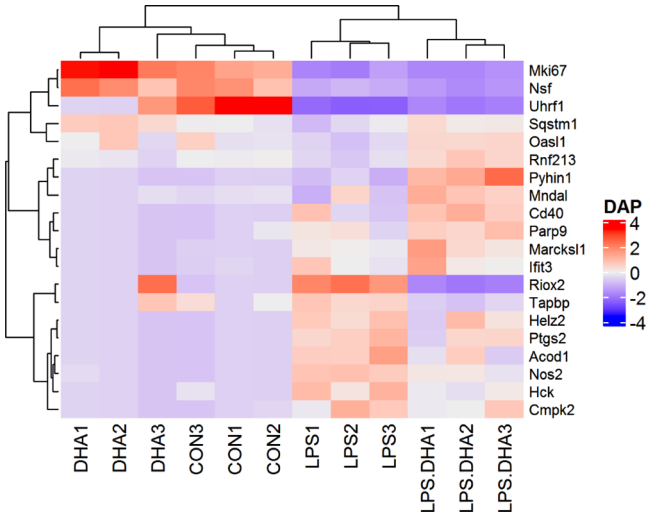

Figure 2. Analysis of altered proteins induced by LPSs and/or DHA at the global level. Hierarchical cluster analysis of DAPs in BV-2 cells. Red indicates a higher relative expression, and purple indicates a lower relative expression. The heat map was generated in R using the 20 DAPs from Table 1 that were significant (BH-corrected $p < 0.05$) with >2 spectra (group average). CON, cells grown under normal conditions; LPS, cells treated with LPSs; DHA, cells treated with DHA; LPS.DHA, cells pretreated with DHA followed by exposure to LPS. The numbers indicate the biological replicates (e.g., CON1 etc.).

PSMs and peptide sequences are 0.1 and 1%, respectively). A total of 2858 proteins with more than one unique peptide were confidently identified and quantified. Using R, we defined 65 DAPs as those with an ANOVA p-value of <0.01 across the four groups (Control, DHA, LPS, and DHA + LPS), and present in at least two of three biological replicates per group. Following Benjamini−Hochberg FDR correction, 26 DAPs were revealed as significantly changed (BH-adjusted p value < 0.05) of which 20 showed a spectral count of >2 (group average). Hierarchical clustering analysis of these 20 DAPs showed relative abundance patterns (Figure 2). There were 17 increases and 6 decreases in DAPs across the four groups (Figure 2 and Table 1). We observed four main trends in abundance of the DAPs (Table 1). The most interesting trend was those proteins that increased in abundance when exposed to LPSs, but are ameliorated by the addition of DHA (i.e., their relative fold-change vs control is lower than with LPS, at control levels, or below control levels, including those not detected in the LPS + DHA group). These proteins represent a number of classes, but the protective effect of DHA is clear in these cases.

The second trend in abundance shown in Table 1 shows increased abundance in response to LPSs but treatment with DHA does not alter their increased expression or afford any protective effects. The third trend in abundance is that related to DHA treatment alone and remains unaffected by LPS or LPS + DHA treatments. Lastly, two proteins show decreased abundance in all groups relative to control; these are involved in ER to Golgi transport and chromatin remodeling.

To gain insight into the functional categories, these DAPs were grouped into three GO categories: biological process (BP), cellular component (CC), and molecular function (MF) (Figure 3). The most dominant BPs represent cellular responses such as immune and defense responses. The prominent cellular compartment categories are cytoplasm, membrane, and nucleus, likely reflecting changes in gene expression and perception of stimuli (LPS + DHA). For MFs, the DAPs are predominantly associated with poly-A RNA and RNA binding (suggesting changes in transcription/translation) and protein kinases (signaling).

PPIs were assessed using the STRING 11.0 database (organism: *M. musculus*). All of the DAPs shown in Figure 2 were analyzed and are represented by 14 proteins shown in Figure 4. Individual proteins are named inside circles. Darker lines show significant relationships between NOS2 and PTGS2, IRG1 and OASL1, OASL1 with both interferon-induced protein with tetratricopeptide repeats 3 (IFIT3) and MMPK2. The IFIT3 protein appears to be a node encompassing a number of interactions with OASL1, CMPK2, PARP9, RNF213, and HELZ2. An outlier group, comprising NSF, VPS11, and SQSTM1 interactions, is also observed.

Many of the DAPs in this PPI map showed increased in abundance when stimulated with LPSs and are then ameliorated by DHA (the first group in Table 1). Some of these proteins are tied to the NF-κB and the Ras/ERK/cPLA$_2$ pathways[33,37] and are discussed further below.

Using GO and PPI analyses, as well as information from the literature,[14,24] the main functional classifications in response to LPS and/or DHA included the NF-κB pathway, fatty acid

https://dx.doi.org/10.1021/acs.jproteome.9b00792
J. Proteome Res. 2020, 19, 2236−2246

Table 1. Log2 Fold-Change of DAPs Across Treatments[a]

accession no.	protein name	gene name	LPS	DHA	LPS + DHA
	Increased in LPSs and Ameliorated by DHA				
P29477	nitric oxide synthase inducible	NOS2	7.28*	n.d.	6.57*
Q3U5Q7	UMP-CMP kinase 2 mito	CMPK2	6.07	n.d.	5.59
P54987	*cis*-aconitate decarboxylase	ACOD1	5.77*	n.d.	4.90*
Q05769	prostaglandin G/H synthase 2	PTGS2	4.77*	n.d.	4.16*
P08103	tyrosine-protein kinase	HCK	4.43	n.d.	3.62
E9QAM5	helicase with zinc finger dom2	HELZ2	4.19*	n.d.	3.66*
Q9R233	tapasin	TAPBP	2.52	−0.62	1.36
Q8CD15	ribosomal oxygenase 2	RIOX2	2.61	n.d.	n.d.
	Increased LPS and LPS + DHA, Unchanged/Lower in DHA				
P28667	MARCKS-related protein	MARKS1	5.36	n.d.	5.56
Q64345	interferon-induced protein with tetratricopeptide repeats 3	IFIT3	4.88	n.d.	4.85
Q8CAS9	polyADP-ribose polymerase 9	PARP9	3.95	n.d.	4.1
P27512	tumor necrosis factor receptor superfamily member 5	CD40	3.94*	n.d.	4.25*
Q8BV49	pyrin and HIN domain-containing protein 1	PYHIN1	3.73*	n.d.	4.95*
D0QMC3	myeloid cell nuclear differentiation antigen-like protein	MNDAL	2.67	n.d.	3.25
Q64337	sequestosome-1	SQSTM1	1.86	0.22	2.02
E9Q555	E3 ubiquitin-protein ligase	RNF213	1.66	−2.01	2.03
Q8VI94	2′-5′-oligoadenylate synthase-like protein 1	OASL1	1.54	−1	1.94
	Increased in DHA, Lower/Unchanged in LPS				
Q3UH60	disco-interacting protein 2-B	DIP2B	n.d.	2.43*	n.d.
Q91W86	vacuolar protein sorting-associated protein 11 homolog	VPS11	n.d.	1.70*	n.d
Q8CHP8	glycerol-3-phosphate phosphatase	PGP	n.d.	0.46	n.d.
Q6PIC6	Na/K-transporting ATPase α-3	AT1A3	−0.11	0.16	−0.3
	Decreased in All Treatments				
P46460	vesicle-fusing ATPase	NSF	−0.93	−1.07	−2.82
E9PVX6	proliferation marker Ki-67	MKI67	−1.85	−0.39	−3.64

[a]NOTES: 1: a positive value indicates increased abundance and a negative value decreased abundance. 2: * indicates imputed fold-change wherein no peptides were detected in the control samples (0 value replaced with 1 for a single replicate). 3: n.d., not detected (no spectral counts were observed in >1 replicate).

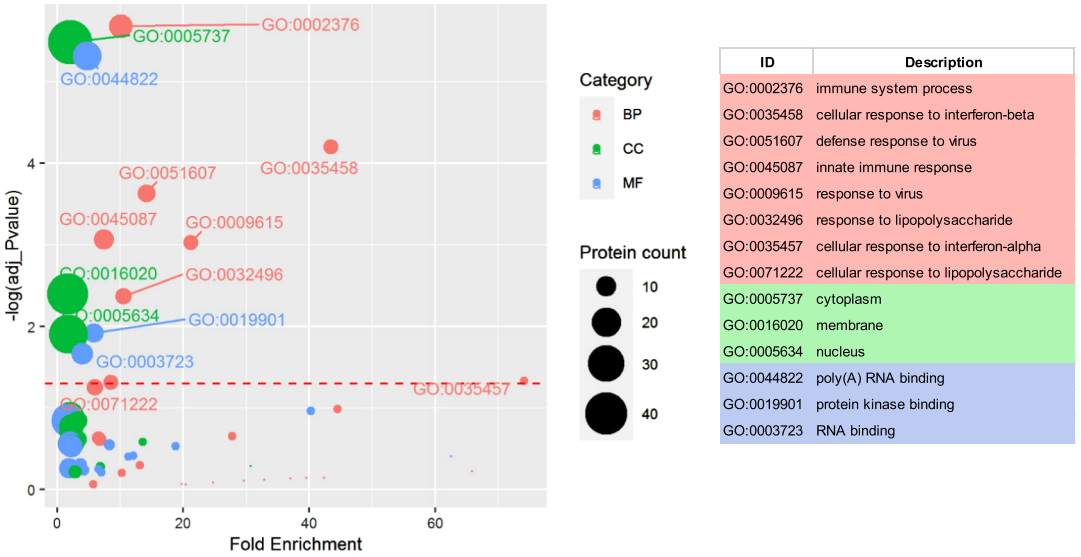

Figure 3. GO enrichment analysis of altered proteins induced by LPSs and/or DHA. The complete list of 65 DAPs (differential at $p < 0.01$, prior to BH correction) were graphed as a bubble plot using R to show GO enrichment. Larger bubbles indicate a higher number of proteins in that GO enrichment category. BP, biological process (red); CC, cellular component (green); MF, molecular function (blue). The dotted line represents the Benjamini corrected $p < 0.05$ threshold, terms above this line are enriched. *X*-axis, fold-enriched GO term; *Y*-axis, −log(adj.-*P*value), Benjamini corrected *p* value.

metabolism, mitochondrial activity, responses to external stimuli, cytoskeleton, DNA binding, and ribosome biogenesis.

3.3. Proteins Involved in the NF-κB Pathway

Studies from our laboratory, as well as others, have demonstrated the effects of endotoxins (such as LPSs) to induce iNOS and proinflammatory cytokines (e.g., TNF-α and IL-1β) in microglial cells.[13,37,38] This study identified proteins, such sequestosome-1 (SQSTM1), nitric oxide synthase (NOS2), and TNF receptor 5 (CD40), which may play important roles in regulating the NF-κB pathway. SQSTM1

https://dx.doi.org/10.1021/acs.jproteome.9b00792
J. Proteome Res. 2020, 19, 2236−2246

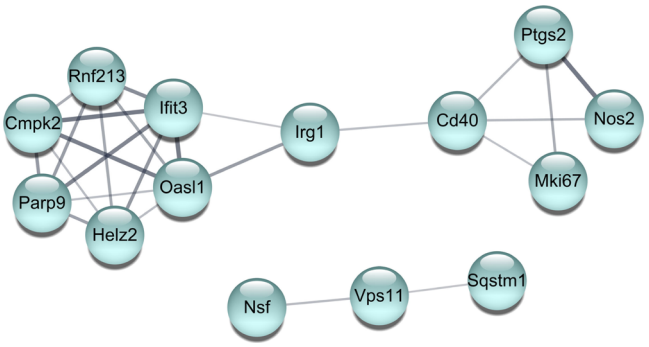

Figure 4. PPI network analysis of altered proteins induced by LPS and/or DHA. The PPI network was constructed using the STRING database version 11.0 with a minimum interaction score of 0.4 (default). The PPI network for 23 DAPs was constructed using cytoscape, with thicker lines indicating stronger interactions. Three clusters were observed.

(also known as the p62 protein) is a signaling adaptor protein, which has been shown genetically and biochemically to activate NF-κB through targeting Ras.[39] The Ras-MAPK pathway is regulated by the Ca^{2+}-dependent RASA4.[40] Induction of iNOS and production of NO are regarded as signature markers of the NF-κB pathway.[8] In the present study, DHA pretreatment decreased the NOS2 expression increased by addition of LPSs (Table 1 and Figure 5B). Compared to the elevated levels of these proteins in cells stimulated with LPSs, the decreased abundance of the same proteins in the DHA + LPS group supports our findings that DHA diminishes the activation of NF-κB by LPSs.[13] In a recent study, LRRC25 has been identified as a novel inhibitor of the NF-κB pathway by targeting NF-κB p65 degradation.[41] In our study, LRRC25 appeared slightly elevated in the LPS and LPS + DHA groups (although below ANOVA $p < 0.01$). The protective effects of DHA are supported by the increased abundance of LRRC25, which suppressed LPS-induced phospho-NF-κB p65 expression in the DHA + LPS group (Figure 5A). Similarly, DHA pretreatment significantly inhibited LPS-induced TNF-α secretion (Figure 5C). In a primary cell model, LGALS9 was shown to enhance microglial TNF-α production by activating the TLR signaling.[42] In our study, LPS stimulation of LGALS9 was observed in ANOVA data ($p < 0.01$) with increased abundance in LPS and slightly

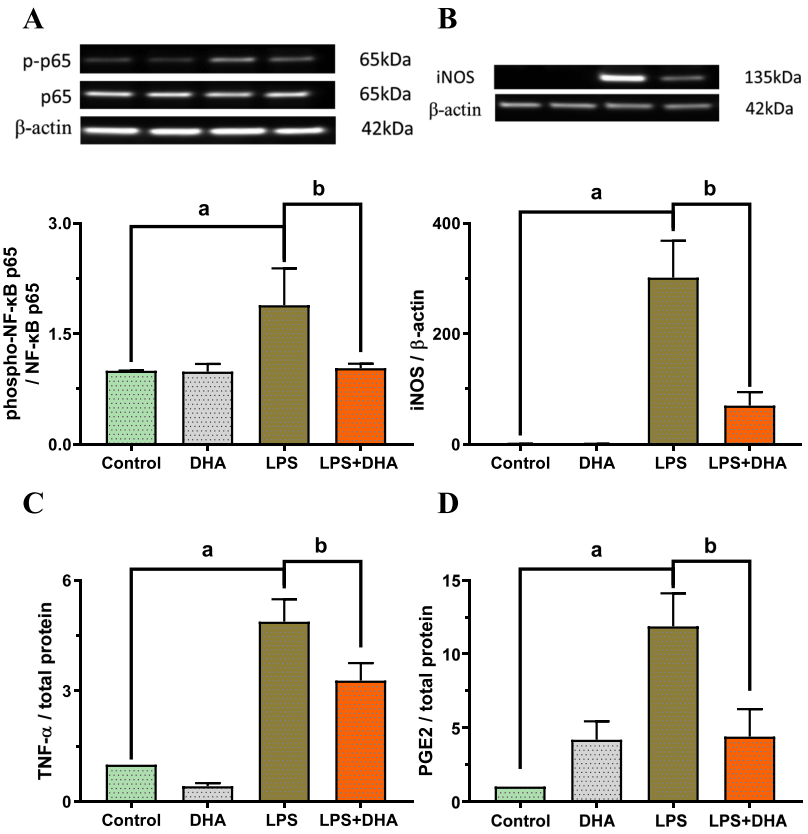

Figure 5. Effects of DHA on LPS-induced phospho-NF-κB p65, iNOS, TNF-α, and PGE2 in BV-2 microglial cells. BV-2 microglial cells were cultured in six-well plates until 90% confluence. After being serum-starved for 3 h, DHA (20 μM) was added for 1 h and cells were stimulated with LPS for 16 h. Cell medium was taken for ELISA assay and cells were lysed for Western blot analysis as described in the text. Representative Western blots are shown in (A,B). The lanes correspond to the plot directly below. Results were obtained from a triplicate assay from a single passage and expressed as mean ± standard deviation ($n = 3$). Repeated experiments with different passages showed similar results. Analysis by one-way ANOVA followed by Tukey's post-tests. (A) Quantification of phospho-NF-κB p65 in BV-2 microglial cells under different treatments, "a" denotes significant differences ($p = 0.0018$) comparing control and LPS; "b" denotes significant differences ($p = 0.0025$) comparing DHA + LPS and LPS. (B) Quantification of iNOS to β-actin ratio in BV-2 microglial cells under different treatments, "a" denotes significant differences ($p < 0.0001$) comparing control and LPS; "b" denotes significant differences ($p < 0.0001$) comparing DHA + LPS and LPS. (C) Quantification of TNF-α in BV-2 microglial cells under different treatments, "a" denotes significant differences ($p < 0.0001$) comparing control and LPS; "b" denotes significant differences ($p < 0.0001$) comparing DHA + LPS and LPS. (D) Quantification of PGE2 in BV-2 microglial cells under different treatments, "a" denotes significant differences ($p = 0.0001$) comparing control and LPS; "b" denotes significant differences ($p = 0.0018$) comparing DHA + LPS and LPS.

https://dx.doi.org/10.1021/acs.jproteome.9b00792
J. Proteome Res. 2020, 19, 2236−2246

attenuated abundance in LPS + DHA (Supplemental Material S3—Table S1). However, the data for this protein did not pass BH correction. Tyrosine-protein kinase (hematopoietic cell kinase, HCK) was increased in the LPS group but less so in the DHA + LPS group. HCK is a myeloid SRC-family kinase known as a pro-survival kinase involved in TLR signaling[43] and has been shown to be rapidly activated in response to LPSs related to chemokine secretions.[44] Tapasin (TAPBP) was increased in the LPS groups, decreased in the DHA group, and its LPS-increased abundance attenuated by DHA in the LPS + DHA group and is associated with the immune response associated with peptide loading on the MHCI complex.[45]

3.4. Proteins Involved in Fatty Acid Metabolism

PUFAs including DHA and ARA are enriched in the phospholipids in the brain.[22] Interestingly, this proteomics study unveiled the ability for DHA treatment to significantly increase several DAPs that are associated with fatty acid metabolism (Figure 6). Therefore, future studies should include investigating the physiological role for these fatty acid-associated proteins. Fish oil diets have been shown to affect the steroid production in adult pig testis.[46]

Different PLA_2s are present in microglial cells and play an important role in regulating the release of PUFAs from the phospholipids.[47] ARA can be metabolized by PTGS2 (COX-2) to produce inflammatory prostaglandins (e.g., PGE2).[48] PTGS2 can bind to nonsteroidal anti-inflammatory drugs, including aspirin and ibuprofen.[49] cAMP-regulated phosphoprotein 19 (ARPP19) is an inhibitor for protein phosphatase 2A (PP2A). Previous findings showed LPSs to induce PP2A activation and consequently increased PTGS2 expression in murine lymphatic endothelial cells.[50] LPSs were also found to induce PTGS2 and microsomal PGE2 synthase through the NF-κB pathway and mitogen-activated protein kinases (MAPKs) in cultured astrocytes.[51] Additionally, treatment of rat astrocytes with DHA could negatively regulate prostaglandin synthesis because of the inhibition of PTGS2.[52] As COX-2 is induced under inflammatory stress, inhibition of COX-2 provides beneficial effects.[53] In our study, prostaglandin G/H synthase 2 (PTGS2/COX-2) significantly increased with LPS treatment (actually not detected in either control or DHA), and this upregulation was diminished by DHA. In order to further confirm this finding, ELISA showed the ability for LPS to increase levels of PGE2, and pretreatment with DHA completely abrogated the LPS-induced increase in PGE2 (Figure 5D).

3.5. Proteins Involved in Response to a Bacterium

Interferon is a mediator of inflammatory responses induced by bacterial endotoxin. Upon stimulation by LPSs, interferon can interact with TLR4 and activate the JAK-STAT signaling pathway, leading to the transcriptional regulation of interferon-stimulated genes (ISGs), which is induced at the transcriptional level through the actions of interferon regulatory factor 3 (IRF3).[54] In this study, several interferon-induced DAPs were increased under LPS treatment. IFIT3 belongs to the group of ISGs, which is induced at the transcriptional level through the actions of IRF3.[55] In a recent study, interferon-activable protein 204 (IFI204) is recognized to be a critical component for canonical LPS-induced TLR4 signaling in mice.[56] E3 ubiquitin-protein ligase DTX3L (DTX3L) and MORC family CW-type zinc finger protein 3 (MORC3) have been implicated in regulating JAK-STAT signaling for interferon signal transduction.[57,58] *cis*-Aconitate decarboxylase (ACOD1/IRG1) is an immunoresponsive anti-inflammatory protein shown to promote endotoxin tolerance related to suppression of pro-inflammatory response.[59] In our study, it was clearly elevated in cells treated with LPS; in fact it was not detected in either control or DHA groups, but this LPS-mediated increase was suppressed in the LPS + DHA group, suggesting a protective effect of DHA. UMP-CMP kinase (CMPK2) is similarly abundant in LPSs and suppressed in the LPS + DHA group and has been shown respond to LPSs and appears to have antiviral properties.[60]

The study here indicated an ability for DHA to suppress the expression of proteins involved in response to a bacterium, further supporting the protective effects of DHA against LPS-induced inflammation.

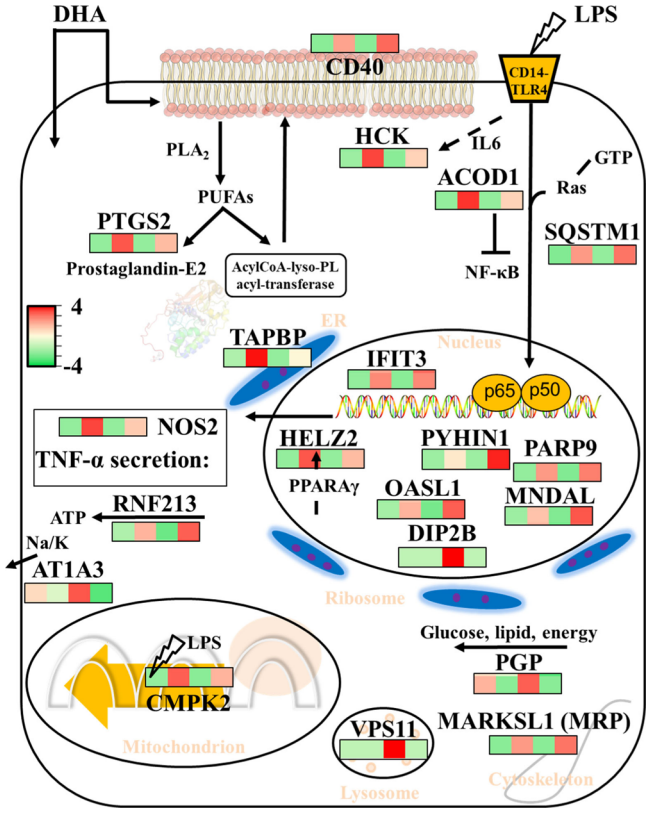

Figure 6. Schematic presentation of key BPs affected by LPS and/or DHA in BV-2 cells. Pathways related to LPS and DHA perception and other downstream cellular processes are shown. Key DAPs' levels are increased (red) and decreased (green) represented by boxes, with the color indicating their $\log_2$ fold-change. The order of the abundance in the boxes are (from left): control, LPS, DHA, and DHA + LPS. Abbreviations: 2′-5′-oligoadenylate synthase-like protein 1, OASL1; *cis*-aconitate decarboxylase, ACOD1; Disco-interacting protein 2-B, DIP2B; E3 ubiquitin-protein ligase, RNF213; glycerol-3-phosphate phosphatase, PGP; helicase with zinc finger domain 2, HELZ2; interferon-induced protein with tetratricopeptide repeats 3, IFIT3; MARCKS-related protein, MARKS1/MRP; myeloid cell nuclear differentiation antigen-like protein, MNDAL; nitric oxide synthase inducible, NOS2; poly[ADP-ribose] polymerase 9, PARP9; prostaglandin G/H synthase 2, PTGS2; pyrin and HIN domain-containing protein 1, PYHIN1; ribosomal oxygenase 2, RIOX2; sequestosome-1, SQSTM1; sodium/potassium-transporting ATPase subunit alpha-3, AT1A3; tapasin, TAPBP; tumor necrosis factor receptor superfamily member 5, CD40; tyrosine-protein kinase, HCK; UMP-CMP kinase 2 mitochondrial, CMPK2; vacuolar protein sorting-associated protein 11 homolog, VPS11.

https://dx.doi.org/10.1021/acs.jproteome.9b00792
J. Proteome Res. 2020, 19, 2236−2246

3.6. Proteins Involved in the Ribosome Function

Ribosomes serve as a complex molecular machine responsible for mediating protein synthesis to maintain cellular homeostasis. There is evidence for LPSs to induce ribosome dysfunction (e.g., mRNA translation).[61] Our results showed the abundance of ribosomal proteins, including ribosomal oxygenase 2 (RIOX2/MINA) and polyADP-ribose polymerase 9 (PARP9), was increased in the LPS group. Some DAPs altered in our LPS-treated microglia cells were also reported from previous proteomic analysis of microglia-derived extracellular vesicles (EVs).[62] In the study by Yang et al.,[62] LPSs were observed to alter secretion of EVs by the activation of ribosomal assembly and translation, which may play a role in the detrimental inflammatory responses in neurodegenerative diseases.

Ribosomal oxygenase 2 (RIOX2/MINA) is a histone lysine demethylase important in TNFb signaling[63] and is associated with cell proliferation in a number of cancers.[64,65] It is increased in the LPS group, but not detected in DHA or the LPS + DHA group, again indicating a protective effect of DHA. Helicase with the zinc-finger domain 2 (HELZ2) is a transcriptional activator of peroxisome proliferator-activated receptor Y[66] which appears to be involved in responses to oxidative stress[67] know to be caused by LPS exposure.

4. CONCLUSIONS

Overall, data from this proteomic study provided details about multiple protein profiles and their corresponding pathways for effects of DHA on LPS-stimulated BV-2 microglial cells (Figure 6). Studies with Western blots and ELISA analysis further confirm the ability for DHA to ameliorate the oxidative and inflammatory responses because of LPSs, including inhibition of the NF-κB pathway, induction of iNOS, and production of TNF-α and PGE2. In addition, this study provided new information regarding the ability of DHA to enhance fatty acid metabolism and altering effects of LPSs on mitochondrial impairments. Taken together, these results form a new basis for therapeutic strategies of DHA against inflammation..

■ ASSOCIATED CONTENT

Supporting Information

The Supporting Information is available free of charge at https://pubs.acs.org/doi/10.1021/acs.jproteome.9b00792.

Cell viability assayed by WST1 from two different cell passages; images of the Western blots used to generate Figure 5 in the paper; correlation coefficients for the three replicates of the four experimental groups; samples 1−3, cells are under normal condition (control samples); samples 4−6, cells are treated with LPSs; samples 7−9, cells are treated with DHA; and samples 10−12, cells are pretreated with DHA followed by LPS (PDF)

Protein abundance data analyzed in R (XLSX)

■ AUTHOR INFORMATION

Corresponding Author

C. Michael Greenlief − *Department of Chemistry and Charles W. Gehrke Proteomics Center, University of Missouri, Columbia 65211, Missouri, United States;* orcid.org/0000-0001-6420-7375; Phone: 573-882-3288; Email: greenliefm@missouri.edu; Fax: 573-882-2754

Authors

Bo Yang − *Department of Chemistry and Charles W. Gehrke Proteomics Center, University of Missouri, Columbia 65211, Missouri, United States*

Runting Li − *Biochemistry Department, University of Missouri, Columbia 65211, Missouri, United States*

Pei N. Liu − *Charles W. Gehrke Proteomics Center, University of Missouri, Columbia 65211, Missouri, United States*

Xue Geng − *Department of Bioengineering, University of Illinois at Chicago, Chicago 60612, Illinois, United States*

Brian P. Mooney − *Biochemistry Department and Charles W. Gehrke Proteomics Center, University of Missouri, Columbia 65211, Missouri, United States*

Chen Chen − *Department of Electrical Engineering and Computer Science, University of Missouri, Columbia 65211, Missouri, United States*

Jianlin Cheng − *Department of Electrical Engineering and Computer Science, University of Missouri, Columbia 65211, Missouri, United States*

Kevin L. Fritsche − *Department of Nutrition and Exercise Physiology, University of Missouri, Columbia 65211, Missouri, United States*

David Q. Beversdorf − *Departments of Radiology, Neurology and Psychological Sciences, and the Thompson Center, University of Missouri, Columbia 65211, Missouri, United States*

James C. Lee − *Department of Bioengineering, University of Illinois at Chicago, Chicago 60612, Illinois, United States;* orcid.org/0000-0002-7173-4875

Grace Y. Sun − *Biochemistry Department, University of Missouri, Columbia 65211, Missouri, United States*

Complete contact information is available at: https://pubs.acs.org/10.1021/acs.jproteome.9b00792

Author Contributions

B.Y., G.Y.S., and C.M.G. conceived the idea and designed the experiments for the project. K.L.F., D.Q.B., B.P.M., and J.C. were involved in the paper preparation. R.L., X.G., P.N.L., C.C., and J.C. provided technical help. All the authors have read/edited and approved the paper.

Funding

This study is supported from the National Science Foundation grant 1726738 (to C.M.G. and B.P.M.), National Institutes of Health grant R01-AG044404 (to J.C.), University of Missouri Research Council grant 17-009 (to D.Q.B.), and the Charles W. Gehrke Proteomics Center FY18 mini grant (to B.Y. and G.Y.S.).

Notes

The authors declare no competing financial interest.

■ ACKNOWLEDGMENTS

We thank Roy Lowery, from the Charles W. Gehrke Proteomics Center at the University of Missouri, for providing assistance with the LC−MS/MS analysis.

■ REFERENCES

(1) Calder, P. C. Omega-3 fatty acids and inflammatory processes. *Nutrients* **2010**, *2*, 355−374.

(2) Hashimoto, M.; Hossain, S.; Al Mamun, A.; Matsuzaki, K.; Arai, H. Docosahexaenoic acid: one molecule diverse functions. *Crit. Rev. Biotechnol.* **2017**, *37*, 579−597.

(3) Oh, D. Y.; Talukdar, S.; Bae, E. J.; Imamura, T.; Morinaga, H.; Fan, W.; Li, P.; Lu, W. J.; Watkins, S. M.; Olefsky, J. M. GPR120 is an omega-3 fatty acid receptor mediating potent anti-inflammatory and insulin-sensitizing effects. *Cell* **2010**, *142*, 687−698.
(4) Bachiller, S.; Jimenez-Ferrer, I.; Paulus, A.; Yang, Y.; Swanberg, M.; Deierborg, T.; Boza-Serrano, A. Microglia in Neurological Diseases: A Road Map to Brain-Disease Dependent-Inflammatory Response. *Front. Cell. Neurosci.* **2018**, *12*, 488.
(5) Zhang, L.; Zhang, J.; You, Z. Switching of the Microglial Activation Phenotype Is a Possible Treatment for Depression Disorder. *Front. Cell. Neurosci.* **2018**, *12*, 306.
(6) McLaughlin, C. N.; Perry-Richardson, J. J.; Coutinho-Budd, J. C.; Broihier, H. T. Dying Neurons Utilize Innate Immune Signaling to Prime Glia for Phagocytosis during Development. *Dev. Cell* **2019**, *48*, 506−522.
(7) Nimmerjahn, A.; Kirchhoff, F.; Helmchen, F. Resting microglial cells are highly dynamic surveillants of brain parenchyma in vivo. *Science* **2005**, *308*, 1314−1318.
(8) Chuang, D. Y.; Simonyi, A.; Kotzbauer, P. T.; Gu, Z.; Sun, G. Y. Cytosolic phospholipase A2 plays a crucial role in ROS/NO signaling during microglial activation through the lipoxygenase pathway. *J. Neuroinflammation* **2015**, *12*, 199.
(9) Sun, G. Y.; Chen, Z.; Jasmer, K. J.; Chuang, D. Y.; Gu, Z.; Hannink, M.; Simonyi, A. Quercetin Attenuates Inflammatory Responses in BV-2 Microglial Cells: Role of MAPKs on the Nrf2 Pathway and Induction of Heme Oxygenase-1. *PLoS One* **2015**, *10*, No. e0141509.
(10) Sun, G. Y.; Li, R.; Cui, J.; Hannink, M.; Gu, Z.; Fritsche, K. L.; Lubahn, D. B.; Simonyi, A. Withania somnifera and Its Withanolides Attenuate Oxidative and Inflammatory Responses and Up-Regulate Antioxidant Responses in BV-2 Microglial Cells. *NeuroMol. Med.* **2016**, *18*, 241−252.
(11) Chuang, D. Y.; Cui, J.; Simonyi, A.; Engel, V. A.; Chen, S.; Fritsche, K. L.; Thomas, A. L.; Applequist, W. L.; Folk, W. R.; Lubahn, D. B.; Sun, A. Y.; Sun, G. Y.; Gu, Z. Dietary Sutherlandia and elderberry mitigate cerebral ischemia-induced neuronal damage and attenuate p47phox and phospho-ERK1/2 expression in microglial cells. *ASN Neuro* **2014**, *6*, 175909141455494.
(12) Sun, G.; Li, R.; Yang, B.; Fritsche, K.; Beversdorf, D.; Lubahn, D.; Geng, X.; Lee, J.; Greenlief, C. Quercetin Potentiates Docosahexaenoic Acid to Suppress Lipopolysaccharide-induced Oxidative/Inflammatory Responses, Alter Lipid Peroxidation Products, and Enhance the Adaptive Stress Pathways in BV-2 Microglial Cells. *Int. J. Mol. Sci.* **2019**, *20*, 932.
(13) Yang, B.; Li, R.; Greenlief, C. M.; Fritsche, K. L.; Gu, Z.; Cui, J.; Lee, J. C.; Beversdorf, D. Q.; Sun, G. Y. Unveiling anti-oxidative and anti-inflammatory effects of docosahexaenoic acid and its lipid peroxidation product on lipopolysaccharide-stimulated BV-2 microglial cells. *J. Neuroinflammation* **2018**, *15*, 202.
(14) Woo, J.; Han, D.; Wang, J. I.; Park, J.; Kim, H.; Kim, Y. Quantitative Proteomics Reveals Temporal Proteomic Changes in Signaling Pathways during BV2 Mouse Microglial Cell Activation. *J. Proteome Res.* **2017**, *16*, 3419−3432.
(15) Bell-Temin, H.; Culver-Cochran, A. E.; Chaput, D.; Carlson, C. M.; Kuehl, M.; Burkhardt, B. R.; Bickford, P. C.; Liu, B.; Stevens, S. M., Jr Novel Molecular Insights into Classical and Alternative Activation States of Microglia as Revealed by Stable Isotope Labeling by Amino Acids in Cell Culture (SILAC)-based Proteomics. *Mol. Cell. Proteomics* **2015**, *14*, 3173−3184.
(16) Andreakos, E.; Sacre, S. M.; Smith, C.; Lundberg, A.; Kiriakidis, S.; Stonehouse, T.; Monaco, C.; Feldmann, M.; Foxwell, B. M. Distinct pathways of LPS-induced NF-κB activation and cytokine production in human myeloid and nonmyeloid cells defined by selective utilization of MyD88 and Mal/TIRAP. *Blood* **2004**, *103*, 2229−2237.
(17) Wijayanti, N.; Huber, S.; Samoylenko, A.; Kietzmann, T.; Immenschuh, S. Role of NF-kB and p38 MAP Kinase Signaling Pathways in the Lipopolysaccharide-Dependent Activation of Heme Oxygenase-1 Gene Expression. *Antioxid. Redox Signaling* **2004**, *6*, 802−810.
(18) Geng, X.; Yang, B.; Li, R.; Teng, T.; Ladu, M. J.; Sun, G. Y.; Greenlief, C. M.; Lee, J. C. Effects of Docosahexaenoic Acid and Its Peroxidation Product on Amyloid-β Peptide-Stimulated Microglia. *Mol. Neurobiol.* **2020**, *57*, 1085.
(19) Sun, G. Y.; Chuang, D. Y.; Zong, Y.; Jiang, J.; Lee, J.; Greenlief, C. M.; Gu, Z.; Simonyi, A. Role of cytosolic phospholipase A2 in oxidative and inflammatory signaling pathways in different cell types in the central nervous system. *Mol. Neurobiol.* **2014**, *50*, 6−14.
(20) Yang, B.; Li, R.; Woo, T.; Browning, J.; Song, H.; Gu, Z.; Cui, J.; Lee, J.; Fritsche, K.; Beversdorf, D.; Sun, G.; Greenlief, C. Maternal Dietary Docosahexaenoic Acid Alters Lipid Peroxidation Products and (n-3)/(n-6) Fatty Acid Balance in Offspring Mice. *Metabolites* **2019**, *9*, 40.
(21) Yang, B.; Fritsche, K. L.; Beversdorf, D. Q.; Gu, Z.; Lee, J. C.; Folk, W. R.; Greenlief, C. M.; Sun, G. Y. Yin-Yang Mechanisms Regulating Lipid Peroxidation of Docosahexaenoic Acid and Arachidonic Acid in the Central Nervous System. *Front. Neurol.* **2019**, *10*, 642.
(22) Sun, G. Y.; Simonyi, A.; Fritsche, K. L.; Chuang, D. Y.; Hannink, M.; Gu, Z.; Greenlief, C. M.; Yao, J. K.; Lee, J. C.; Beversdorf, D. Q. Docosahexaenoic acid (DHA): An essential nutrient and a nutraceutical for brain health and diseases. *Prostaglandins, Leukotrienes Essent. Fatty Acids* **2018**, *136*, 3−13.
(23) Shalini, S.-M.; Ho, C. F.-Y.; Ng, Y.-K.; Tong, J.-X.; Ong, E.-S.; Herr, D. R.; Dawe, G. S.; Ong, W.-Y. Distribution of Alox15 in the Rat Brain and Its Role in Prefrontal Cortical Resolvin D1 Formation and Spatial Working Memory. *Mol. Neurobiol.* **2018**, *55*, 1537−1550.
(24) Ortea, I.; González-Fernández, M. J.; Ramos-Bueno, R. P.; Guil-Guerrero, J. L. Proteomics Study Reveals That Docosahexaenoic and Arachidonic Acids Exert Different In Vitro Anticancer Activities in Colorectal Cancer Cells. *J. Agric. Food Chem.* **2018**, *66*, 6003−6012.
(25) Zheng, X.; Wojcik, R.; Zhang, X.; Ibrahim, Y. M.; Burnum-Johnson, K. E.; Orton, D. J.; Monroe, M. E.; Moore, R. J.; Smith, R. D.; Baker, E. S. Coupling Front-End Separations, Ion Mobility Spectrometry, and Mass Spectrometry For Enhanced Multidimensional Biological and Environmental Analyses. *Annu. Rev. Anal. Chem.* **2017**, *10*, 71−92.
(26) Meier, F.; Brunner, A.-D.; Koch, S.; Koch, H.; Lubeck, M.; Krause, M.; Goedecke, N.; Decker, J.; Kosinski, T.; Park, M. A.; Bache, N.; Hoerning, O.; Cox, J.; Räther, O.; Mann, M. Online Parallel Accumulation-Serial Fragmentation (PASEF) with a Novel Trapped Ion Mobility Mass Spectrometer. *Mol. Cell. Proteomics* **2018**, *17*, 2534−2545.
(27) Meier, F.; Beck, S.; Grassl, N.; Lubeck, M.; Park, M. A.; Raether, O.; Mann, M. Parallel Accumulation-Serial Fragmentation (PASEF): Multiplying Sequencing Speed and Sensitivity by Synchronized Scans in a Trapped Ion Mobility Device. *J. Proteome Res.* **2015**, *14*, 5378−5387.
(28) Shen, S.; Yu, S.; Binek, J.; Chalimoniuk, M.; Zhang, X.; Lo, S.-C.; Hannink, M.; Wu, J.; Fritsche, K.; Donato, R.; Sun, G. Y. Distinct signaling pathways for induction of type II NOS by IFNgamma and LPS in BV-2 microglial cells. *Neurochem. Int.* **2005**, *47*, 298−307.
(29) Ni, Y.; Teng, T.; Li, R.; Simonyi, A.; Sun, G. Y.; Lee, J. C. TNFalpha alters occludin and cerebral endothelial permeability: Role of p38MAPK. *PLoS One* **2017**, *12*, No. e0170346.
(30) Yang, B.; Thomas, A.; Greenlief, C. Comparative Proteomic Analysis Unveils Critical Pathways Underlying the Role of Nitrogen Fertilizer Treatment in American Elderberry. *Proteomes* **2019**, *7*, 10.
(31) Beck, S.; Michalski, A.; Raether, O.; Lubeck, M.; Kaspar, S.; Goedecke, N.; Baessmann, C.; Hornburg, D.; Meier, F.; Paron, I.; Kulak, N. A.; Cox, J.; Mann, M. The Impact II, a Very High-Resolution Quadrupole Time-of-Flight Instrument (QTOF) for Deep Shotgun Proteomics. *Mol. Cell. Proteomics* **2015**, *14*, 2014−2029.
(32) Zhang, J.; Xin, L.; Shan, B.; Chen, W.; Xie, M.; Yuen, D.; Zhang, W.; Zhang, Z.; Lajoie, G. A.; Ma, B. PEAKS DB: de novo sequencing assisted database search for sensitive and accurate peptide identification. *Mol. Cell. Proteomics* **2012**, *11*, M111.010587.

https://dx.doi.org/10.1021/acs.jproteome.9b00792
J. Proteome Res. 2020, 19, 2236−2246

(33) Huang, D. W.; Sherman, B. T.; Lempicki, R. A. Bioinformatics enrichment tools: paths toward the comprehensive functional analysis of large gene lists. *Nucleic Acids Res.* **2008**, *37*, 1−13.
(34) Szklarczyk, D.; Gable, A. L.; Lyon, D.; Junge, A.; Wyder, S.; Huerta-Cepas, J.; Simonovic, M.; Doncheva, N. T.; Morris, J. H.; Bork, P.; Jensen, L. J.; Mering, C. v. STRING v11: protein−protein association networks with increased coverage, supporting functional discovery in genome-wide experimental datasets. *Nucleic Acids Res.* **2018**, *47*, D607−D613.
(35) Shannon, P.; Markiel, A.; Ozier, O.; Baliga, N. S.; Wang, J. T.; Ramage, D.; Amin, N.; Schwikowski, B.; Ideker, T. Cytoscape: A Software Environment for Integrated Models of Biomolecular Interaction Networks. *Genome Res.* **2003**, *13*, 2498−2504.
(36) Vizcaíno, J. A.; Deutsch, E. W.; Wang, R.; Csordas, A.; Reisinger, F.; Ríos, D.; Dianes, J. A.; Sun, Z.; Farrah, T.; Bandeira, N.; Binz, P.-A.; Xenarios, I.; Eisenacher, M.; Mayer, G.; Gatto, L.; Campos, A.; Chalkley, R. J.; Kraus, H.-J.; Albar, J. P.; Martinez-Bartolomé, S.; Apweiler, R.; Omenn, G. S.; Martens, L.; Jones, A. R.; Hermjakob, H. ProteomeXchange provides globally coordinated proteomics data submission and dissemination. *Nat. Biotechnol.* **2014**, *32*, 223−226.
(37) Sheng, W.; Zong, Y.; Mohammad, A.; Ajit, D.; Cui, J.; Han, D.; Hamilton, J. L.; Simonyi, A.; Sun, A. Y.; Gu, Z.; Hong, J.-S.; Weisman, G. A.; Sun, G. Y. Pro-inflammatory cytokines and lipopolysaccharide induce changes in cell morphology, and upregulation of ERK1/2, iNOS and sPLA(2)-IIA expression in astrocytes and microglia. *J. Neuroinflammation* **2011**, *8*, 121.
(38) Rossol, M.; Heine, H.; Meusch, U.; Quandt, D.; Klein, C.; Sweet, M. J.; Hauschildt, S. LPS-induced cytokine production in human monocytes and macrophages. *Crit. Rev. Immunol.* **2011**, *31*, 379−446.
(39) Duran, A.; Linares, J. F.; Galvez, A. S.; Wikenheiser, K.; Flores, J. M.; Diaz-Meco, M. T.; Moscat, J. The signaling adaptor p62 is an important NF-kappaB mediator in tumorigenesis. *Cancer Cell* **2008**, *13*, 343−354.
(40) Lockyer, P. J.; Kupzig, S.; Cullen, P. J. CAPRI regulates Ca(2+)-dependent inactivation of the Ras-MAPK pathway. *Curr. Biol.* **2001**, *11*, 981−986.
(41) Feng, Y.; Duan, T.; Du, Y.; Jin, S.; Wang, M.; Cui, J.; Wang, R. F. LRRC25 Functions as an Inhibitor of NF-kappaB Signaling Pathway by Promoting p65/RelA for Autophagic Degradation. *Sci. Rep.* **2017**, *7*, 13448.
(42) Steelman, A. J.; Li, J. Astrocyte galectin-9 potentiates microglial TNF secretion. *J. Neuroinflammation* **2014**, *11*, 144.
(43) Liu, X.; Chen, J. G.; Munshi, M.; Hunter, Z. R.; Xu, L.; Kofides, A.; Tsakmaklis, N.; Demos, M. G.; Guerrera, M. L.; Chan, G. G.; Jimenez, C.; Patterson, C. J.; Meid, K.; Keezer, A.; Castillo, J. J.; Treon, S. P.; Yang, G. Expression of the prosurvival kinase HCK requires PAX5 and mutated MYD88 signaling in MYD88-driven B-cell lymphomas. *Blood Adv.* **2020**, *4*, 141−153.
(44) Mazzi, P.; Caveggion, E.; Lapinet-Vera, J. A.; Lowell, C. A.; Berton, G. The Src-Family Kinases Hck and Fgr Regulate Early Lipopolysaccharide-Induced Myeloid Cell Recruitment into the Lung and Their Ability To Secrete Chemokines. *J. Immunol.* **2015**, *195*, 2383−2395.
(45) Fisette, O.; Wingbermühle, S.; Tampé, R.; Schäfer, L. V. Molecular mechanism of peptide editing in the tapasin−MHC I complex. *Sci. Rep.* **2016**, *6*, 19085.
(46) Castellano, C.-A.; Audet, I.; Laforest, J.-P.; Matte, J. J.; Suh, M. Fish oil diets alter the phospholipid balance, fatty acid composition, and steroid hormone concentrations in testes of adult pigs. *Theriogenology* **2011**, *76*, 1134−1145.
(47) Sun, G. Y.; Xu, J.; Jensen, M. D.; Simonyi, A. Phospholipase A2 in the central nervous system: implications for neurodegenerative diseases. *J. Lipid Res.* **2004**, *45*, 205−213.
(48) Ricciotti, E.; FitzGerald, G. A. Prostaglandins and inflammation. *Arterioscler., Thromb., Vasc. Biol.* **2011**, *31*, 986−1000.
(49) Zarghi, A.; Arfaei, S. Selective COX-2 Inhibitors: A Review of Their Structure-Activity Relationships. *Iran. J. Pharm. Res.* **2011**, *10*, 655.
(50) Chuang, Y.-F.; Chen, M.-C.; Huang, S.-W.; Hsu, Y.-F.; Ou, G.; Tsai, Y.-J.; Hsu, M.-J. Protein Phosphatase 2A in Lipopolysaccharide-Induced Cyclooxygenase-2 Expression in Murine Lymphatic Endothelial Cells. *PLoS One* **2015**, *10*, No. e0137177.
(51) Font-Nieves, M.; Sans-Fons, M. G.; Gorina, R.; Bonfill-Teixidor, E.; Salas-Pérdomo, A.; Márquez-Kisinousky, L.; Santalucia, T.; Planas, A. M. Induction of COX-2 enzyme and down-regulation of COX-1 expression by lipopolysaccharide (LPS) control prostaglandin E2 production in astrocytes. *J. Biol. Chem.* **2012**, *287*, 6454−6468.
(52) Strokin, M.; Sergeeva, M.; Reiser, G. Prostaglandin synthesis in rat brain astrocytes is under the control of the n-3 docosahexaenoic acid, released by group VIB calcium-independent phospholipase A2. *J. Neurochem.* **2007**, *102*, 1771−1782.
(53) Araki, E.; Forster, C.; Dubinsky, J. M.; Ross, M. E.; Iadecola, C. Cyclooxygenase-2 inhibitor ns-398 protects neuronal cultures from lipopolysaccharide-induced neurotoxicity. *Stroke* **2001**, *32*, 2370−2375.
(54) Schneider, W. M.; Chevillotte, M. D.; Rice, C. M. Interferon-stimulated genes: a complex web of host defenses. *Annu. Rev. Immunol.* **2014**, *32*, 513−545.
(55) Diamond, M. S.; Farzan, M. The broad-spectrum antiviral functions of IFIT and IFITM proteins. *Nat. Rev. Immunol.* **2013**, *13*, 46−57.
(56) Yi, Y.-S.; Jian, J.; Gonzalez-Gugel, E.; Shi, Y.-X.; Tian, Q.; Fu, W.; Hettinghouse, A.; Song, W.; Liu, R.; He, M.; Qi, H.; Yang, J.; Du, X.; Xiao, G.; Chen, L.; Liu, C.-j. p204 Is Required for Canonical Lipopolysaccharide-induced TLR4 Signaling in Mice. *EBioMedicine* **2018**, *29*, 78−91.
(57) Zhang, Y.; Mao, D.; Roswit, W. T.; Jin, X.; Patel, A. C.; Patel, D. A.; Agapov, E.; Wang, Z.; Tidwell, R. M.; Atkinson, J. J.; Huang, G.; McCarthy, R.; Yu, J.; Yun, N. E.; Paessler, S.; Lawson, T. G.; Omattage, N. S.; Brett, T. J.; Holtzman, M. J. PARP9-DTX3L ubiquitin ligase targets host histone H2BJ and viral 3C protease to enhance interferon signaling and control viral infection. *Nat. Immunol.* **2015**, *16*, 1215−1227.
(58) Ling, K.-H.; Hewitt, C. A.; Tan, K.-L.; Cheah, P.-S.; Vidyadaran, S.; Lai, M.-I.; Lee, H.-C.; Simpson, K.; Hyde, L.; Pritchard, M. A.; Smyth, G. K.; Thomas, T.; Scott, H. S. Functional transcriptome analysis of the postnatal brain of the Ts1Cje mouse model for Down syndrome reveals global disruption of interferon-related molecular networks. *BMC Genomics* **2014**, *15*, 624.
(59) Li, Y.; Zhang, P.; Wang, C.; Han, C.; Meng, J.; Liu, X.; Xu, S.; Li, N.; Wang, Q.; Shi, X.; Cao, X. Immune Responsive Gene 1 (IRG1) Promotes Endotoxin Tolerance by Increasing A20 Expression in Macrophages through Reactive Oxygen Species. *J. Biol. Chem.* **2013**, *288*, 16225−16234.
(60) Liu, W.; Chen, B.; Chen li, l.; Yao, J.; Liu, J.; Kuang, M.; Wang, F.; Wang, Y.; Elkady, G.; Lu, Y.; Zhang, Y.; Liu, X. Identification of fish CMPK2 as an interferon stimulated gene against SVCV infection. *Fish Shellfish Immunol.* **2019**, *92*, 125−132.
(61) Ceppi, M.; Clavarino, G.; Gatti, E.; Schmidt, E. K.; de Gassart, A.; Blankenship, D.; Ogola, G.; Banchereau, J.; Chaussabel, D.; Pierre, P. Ribosomal protein mRNAs are translationally-regulated during human dendritic cells activation by LPS. *Immunome Res.* **2009**, *5*, 5.
(62) Yang, Y.; Boza-Serrano, A.; Dunning, C. J. R.; Clausen, B. H.; Lambertsen, K. L.; Deierborg, T. Inflammation leads to distinct populations of extracellular vesicles from microglia. *J. Neuroinflammation* **2018**, *15*, 168.
(63) Lian, S. L.; Mihi, B.; Koyanagi, M.; Nakayama, T.; Bix, M. A SNP uncoupling Mina expression from the TGFβ signaling pathway. *Immun., Inflammation Dis.* **2018**, *6*, 58−71.
(64) Zhou, L.; Zhang, T.; Zhu, Q.; Zhang, P.; Yu, L.; Shen, B.; Yi, W.; Qiu, M.; Zhu, C. Mina53 regulates the differentiation and proliferation of leukemia cells. *Hematol. Oncol.* **2019**, *37*, 513−515.
(65) Xuan, F.; Huang, M.; Zhao, E.; Cui, H. MINA53 deficiency leads to glioblastoma cell apoptosis via inducing DNA replication stress and diminishing DNA damage response. *Cell Death Dis.* **2018**, *9*, 1062.
(66) Katano-Toki, A.; Satoh, T.; Tomaru, T.; Yoshino, S.; Ishizuka, T.; Ishii, S.; Ozawa, A.; Shibusawa, N.; Tsuchiya, T.; Saito, T.; Shimizu, H.;

https://dx.doi.org/10.1021/acs.jproteome.9b00792
J. Proteome Res. 2020, 19, 2236−2246

Hashimoto, K.; Okada, S.; Yamada, M.; Mori, M. THRAP3 Interacts with HELZ2 and Plays a Novel Role in Adipocyte Differentiation. *Mol. Endocrinol.* **2013**, *27*, 769−780.
(67) Uddin, M. S.; Kabir, M. T.; Jakaria, M.; Mamun, A. A.; Niaz, K.; Amran, M. S.; Barreto, G. E.; Ashraf, G. M. Endothelial PPARγ Is Crucial for Averting Age-Related Vascular Dysfunction by Stalling Oxidative Stress and ROCK. *Neurotoxic. Res.* **2019**, *36*, 583−601.

https://dx.doi.org/10.1021/acs.jproteome.9b00792
J. Proteome Res. 2020, 19, 2236−2246